Two-dimensional intrinsic ferromagnetic monolayer transition metal oxyhydroxide -Supplemental Material-

Hongyu Chen,[1] Peizhe Tang,[2,3] and Jia Li[1,4]

[1] *Institute of Materials Research, Tsinghua Shenzhen International Graduate School, Tsinghua University, Shenzhen 518055, China*
[2] *School of Materials Science and Engineering, Beihang University, Beijing 100191, China*
[3] *Max Planck Institute for the Structure and Dynamics of Matter, Center for Free Electron Laser Science, 22761 Hamburg, Germany*
[4] *Guangdong Provincial Key Laboratory of Thermal Management Engineering and Materials, Tsinghua Shenzhen International Graduate School, Tsinghua University, Shenzhen 518055, China*

(Dated: April 23, 2021)

CONTENTS

Phonon calculations for monolayer TMOOHs (TM = V, Cr, Mn, Co, Ni) 2
Convergence-test of the imaginary frequencies around Γ point 2
Partial density of states of phonon spectra 2

Energy-band calculations for monolayer VOOH and CrOOH 3
Energy bands and partial bands for monolayer VOOH and CrOOH 3
More accurate bandgaps using HSE06 functional 3

Derivation process of the expression of d-orbitals 4

Evaluation of T_C 7

References 8

PHONON CALCULATIONS FOR MONOLAYER TMOOHS (TM = V, CR, MN, CO, NI)

Convergence-test of the imaginary frequencies around Γ point

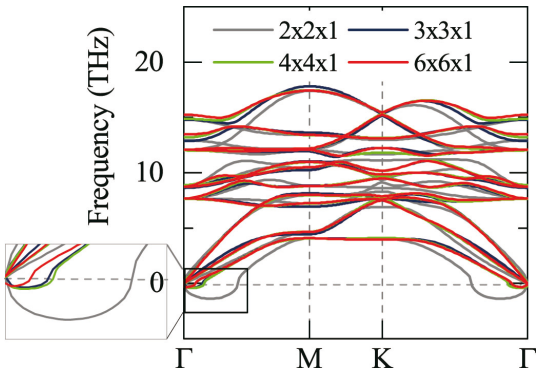

FIG. S1. Phonon spectra of monolayer VOOH using supercells with size of 2 × 2 × 1, 3 × 3 × 1, 4 × 4 × 1, 6 × 6 × 1. The small packet around Γ point shrinks as supercell get larger, which means that it is from the numerical error, not structural unstability.

Partial density of states of phonon spectra

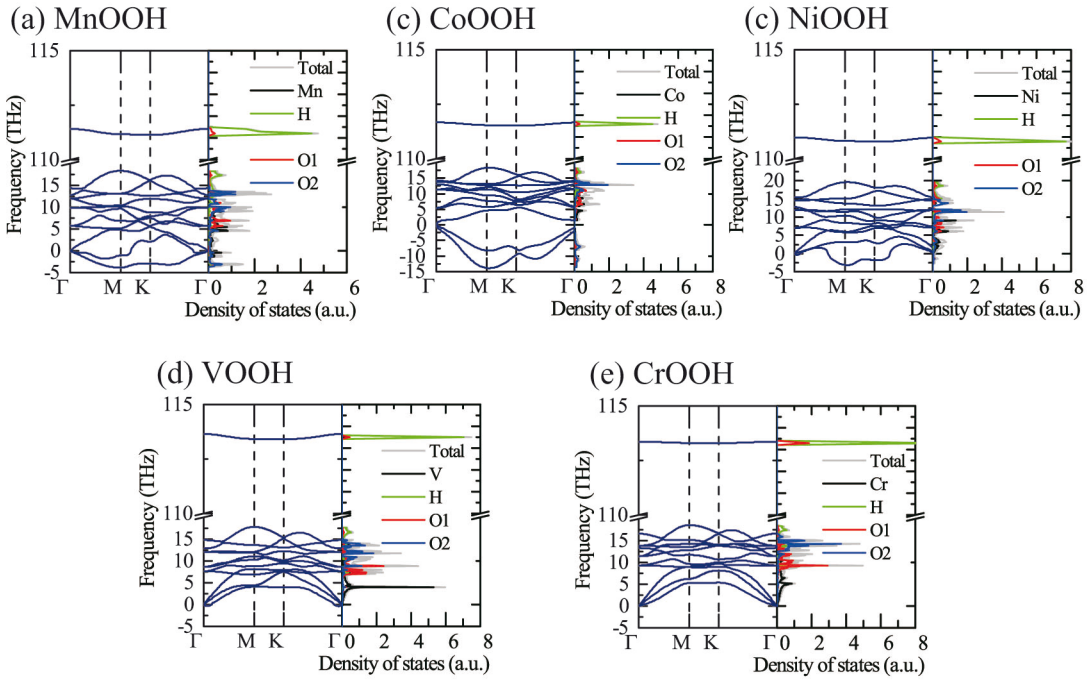

FIG. S2. Phonon spectra of monolayer TMOOHs (TM = V, Cr, Mn, Co, Ni) and their partial density of states using 3 × 3 × 1 supercells. For monolayer VOOH and CrOOH, there is no imaginary frequency in the whole Brillouin zone, apart from a small packet around Γ point for VOOH. For monolayer MnOOH, CoOOH and NiOOH, there are considerable imaginary frequencies in the acoustic branch, which means that they are not dynamically stable.

ENERGY-BAND CALCULATIONS FOR MONOLAYER VOOH AND CROOH

Energy bands and partial bands for monolayer VOOH and CrOOH

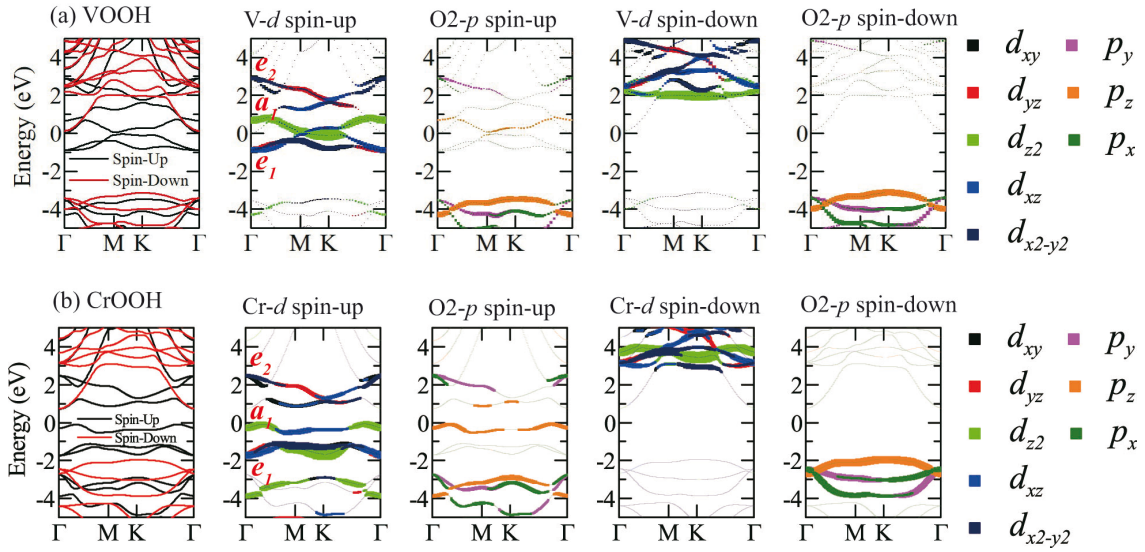

FIG. S3. Band structures and partial bands using the GGA+U method for monolayer (a) VOOH and (b) CrOOH, respectively, where monolayer VOOH and CrOOH are both semiconductors. The d orbitals of transition metal atoms are all around the Fermi level. Besides, these d orbitals split into three groups, a_1, e_1, and e_2, at the Γ point, and a_1 orbital is ascribed to d_{z^2} orbitals. Further, there is strong hybridization between unoccupied V-a_1 and occupied O2-p_z orbitals and between unoccupied Cr-e_2 and occupied O2-$p_{x/y}$ orbitals in the spin-up channel around the Fermi level.

More accurate bandgaps using HSE06 functional

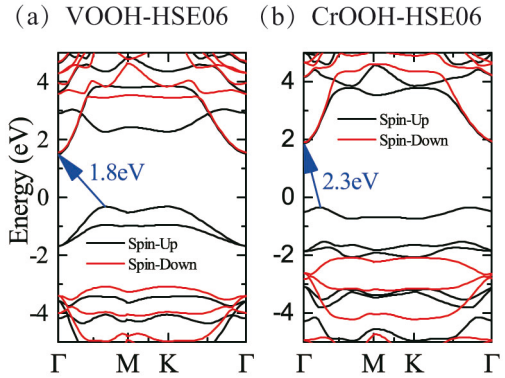

FIG. S4. Energy bands using HSE06 functional for monolayer (a) VOOH and (b) CrOOH.

DERIVATION PROCESS OF THE EXPRESSION OF d-ORBITALS

According to transition-metal-ion theory [1], transition metal atom surrounded by nonmetallic atoms could be considered as one cation. Further, based on crystal field theory [2], the influence of anions on the energy-level splitting of d-electrons of cations could be investigated using the first-order perturbation method. Under the single-electron approximation [2], the matrix elements of first-order perturbation Hamiltonian could be $H_{i,j} =< \phi_i|H_1|\phi_j >$, where H_1 represents the crystal field potential, dependent on the local symmetry in the corresponding point group (namely, the geometric coordination environment of transition metal cations). The wavefunctions of d orbitals $\{\phi_i\}$ (i =1, 2, 3, 4, 5) could be expressed by spherical harmonics Y_{lm}, where $l = 2$ and m = -2, -1, 0, 1, 2, are the angular and magnetic quantum number, respectively.

Conveniently, if $\{\phi_i\}$ are the bases of corresponding point group's irreducible representation, the first-order perturbation matrix will be diagonalized. Consequently $\{\phi_i\}$ become the first-order perturbation matrix's eigenfunctions, namely, representing the eigenstates under the crystal-field potential. This condition or process, is also called "symmetry-adapting" [3]. Usually, we choose five orthogonal linear combinations of Y_{lm} as the bases, in the premise of that, one split level do not mix with other split levels under corresponding the symmetry-transformation. This premise brings the crystal field potential, H_{ij}, into block form according to the irreducible representation in the point group for the corresponding angular quantum number, such as A_1+2E in C_{3v} for $l = 2$. For the one-dimensional irreducible representation, the base is the eigenfunction, and for the two-dimensional irreducible representation, eigenfunctions are linear combinations of the two bases.

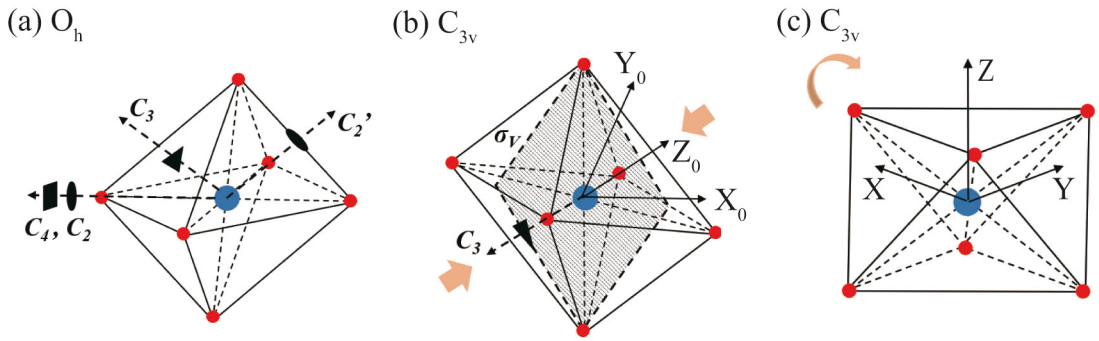

FIG. S5. (a) Schematic representation of octahedron (point group O_h) with its symmetry operation. (b) Schematic representation of C_{3v} crystal field in XYZ coordinates where [111]-direction is along the C_3 rotation axis. (c) Schematic representation of C_{3v} crystal field in XYZ coordinates, where Z-axis is along the C_3 rotation axis. The blue and red balls represent cations and anions, respectively. In our work, the higher-lying e double-degenerated states are unoccupied for monolayer VOOH and CrOOH, which should be included to analyze the superexchange interaction between V/Cr-d orbitals and O-p orbitals. Besides, to explain the origin of the easy-plane or easy-axis magnetic anisotropy in a two-dimensional lattice, we need the expressions of d orbitals substituted into the spin-orbit coupling (SOC) induced magnetic anisotropy energy (MAE). Thus, we should revise the expressions of wave functions of d orbitals in XYZ coordinates, where the Z-axis is along the C_3 rotation axis as shown in Fig. S5(c).

For the C$_{3v}$ crystal-field potential [see Fig. S5(b)], it could be viewed as the distorted O_h crystal field [see Fig. S5(a) to Fig. S5(b)], where only three kinds of symmetry operations remain ($1E$, $2C_3$, $3\sigma_v$). We firstly establish a coordinate set as shown in Fig. S5(b) to make it simple to transform spherical harmonics under C_3 operation. The transformation of there basis functions under the symmetry operations in C_{3v} is shown in Table S1. And these basis functions can be expressed by a linear combination of spherical harmonics as following:

$$a_1^0 : i\sqrt{\frac{1}{6}}((d_1 + d_{-1} - d_2 + d_{-2}) + i(d_1 - d_{-1})) = \sqrt{\frac{1}{3}}(d_{yz} + d_{xz} + d_{xy}) \tag{1}$$

$$e_1^0 \begin{cases} e_{a1}^0 : d_0 = d_{z^2} \\ e_{b1}^0 : \sqrt{\frac{1}{2}}(d_2 + d_{-2}) = d_{x^2-y^2} \end{cases} \tag{2}$$

$$e_2^0 \begin{cases} e_{a2}^0 : \sqrt{\frac{1}{12}}((d_1 - d_{-1}) - i(d_1 + d_{-1} + 2d_2 - 2d_{-2})) = \sqrt{\frac{1}{6}}(-d_{xz} - d_{yz} + 2d_{xy}) \\ e_{b2}^0 : \sqrt{\frac{1}{4}}((d_1 - d_{-1}) + i(d_1 + d_{-1})) = \sqrt{\frac{1}{2}}(-d_{xz} + d_{yz}) \end{cases} \tag{3}$$

TABLE S1. Transformation of d-orbital functions under symmetry operation in C_{3v} point group. d_i (i = 2, 1, 0, -1, -2) represent the spherical harmonics, $Y_{2,\pm 2} = \sqrt{\frac{5}{4\pi}} \times \sqrt{\frac{3}{8}}\ \frac{(x \pm iy)^2}{r^2}$, $Y_{2,\pm 1} = \mp \sqrt{\frac{5}{4\pi}} \times \sqrt{\frac{3}{2}}\ \frac{z(x \pm iy)}{r^2}$, $Y_{2,0} = \sqrt{\frac{5}{4\pi}} \times \sqrt{\frac{1}{4}}\ \frac{3z^2 - r^2}{r^2}$. χ is the corresponding character for the bases and symmetry transformation in this case.

	E	$C_3 \begin{cases} x \to y \\ y \to z \\ z \to x \end{cases}$	$\sigma_v \begin{cases} x \to y \\ y \to x \\ z \to z \end{cases}$
d_2	d_2	$-\sqrt{\frac{6}{16}}d_0 - \sqrt{\frac{1}{16}}d_2 - \sqrt{\frac{1}{16}}d_{-2} - \sqrt{\frac{4}{16}}d_1 - \sqrt{\frac{4}{16}}d_{-1}$	$-d_{-2}$
d_1	d_1	$\frac{i}{2}d_2 - \frac{i}{2}d_{-2} + \frac{i}{2}d_1 - \frac{i}{2}d_{-1}$	$-id_{-1}$
d_0	d_0	$-\sqrt{\frac{2}{8}}d_0 + \sqrt{\frac{3}{8}}d_2 + \sqrt{\frac{3}{8}}d_{-2}$	d_0
d_{-1}	d_{-1}	$-\frac{i}{2}d_2 + \frac{i}{2}d_{-2} + \frac{i}{2}d_1 - \frac{i}{2}d_{-1}$	id_1
d_{-2}	d_{-2}	$-\sqrt{\frac{6}{16}}d_0 - \sqrt{\frac{1}{16}}d_2 - \sqrt{\frac{1}{16}}d_{-2} + \sqrt{\frac{4}{16}}d_1 + \sqrt{\frac{4}{16}}d_{-1}$	$-d_2$
χ	5	-1	1

These linear combinations possess the transformation under the symmetry operations according to C_{3v} point group as following:

$$P_{C_3}\sqrt{\frac{1}{3}}(d_{yz} + d_{xz} + d_{xy}) = \sqrt{\frac{1}{3}}(d_{yz} + d_{xz} + d_{xy}) \tag{4}$$

$$P_{C_3}\begin{bmatrix} d_{z^2} \\ d_{x^2-y^2} \end{bmatrix} = \begin{bmatrix} -\frac{1}{2} & \frac{\sqrt{3}}{2} \\ -\frac{\sqrt{3}}{2} & -\frac{1}{2} \end{bmatrix}\begin{bmatrix} d_{z^2} \\ d_{x^2-y^2} \end{bmatrix} \tag{5}$$

$$P_{C_3}\begin{bmatrix} \sqrt{\frac{1}{6}}(-d_{xz} - d_{yz} + 2d_{xy}) \\ \sqrt{\frac{1}{2}}(-d_{xz} + d_{yz}) \end{bmatrix} = \begin{bmatrix} -\frac{1}{2} & \frac{\sqrt{3}}{2} \\ -\frac{\sqrt{3}}{2} & -\frac{1}{2} \end{bmatrix}\begin{bmatrix} \sqrt{\frac{1}{6}}(-d_{xz} - d_{yz} + 2d_{xy}) \\ \sqrt{\frac{1}{2}}(-d_{xz} + d_{yz}) \end{bmatrix} \tag{6}$$

$$P_{\sigma_v}\sqrt{\frac{1}{3}}(d_{yz} + d_{xz} + d_{xy}) = \sqrt{\frac{1}{3}}(d_{yz} + d_{xz} + d_{xy}) \tag{7}$$

$$P_{\sigma_v}\begin{bmatrix} d_{z^2} \\ d_{x^2-y^2} \end{bmatrix} = \begin{bmatrix} 1 & 0 \\ 0 & -1 \end{bmatrix}\begin{bmatrix} d_{z^2} \\ d_{x^2-y^2} \end{bmatrix} \tag{8}$$

$$P_{\sigma_v}\begin{bmatrix} \sqrt{\frac{1}{6}}(-d_{xz} - d_{yz} + 2d_{xy}) \\ \sqrt{\frac{1}{2}}(-d_{xz} + d_{yz}) \end{bmatrix} = \begin{bmatrix} 1 & 0 \\ 0 & -1 \end{bmatrix}\begin{bmatrix} \sqrt{\frac{1}{6}}(-d_{xz} - d_{yz} + 2d_{xy}) \\ \sqrt{\frac{1}{2}}(-d_{xz} + d_{yz}) \end{bmatrix} \tag{9}$$

where P_{C_3} and P_{σ_v} represent the symmetry operation in C_{3v} point group as shown in Table S2. It can be seen that these linear combinations (a_1 and $2e$) do not mix with each other, which means that they are a set of appropriate orthogonal bases to bring H_{ij} into block form according to the irreducible representations of C_{3v} point group point

group for l =2. Further, to get a set of basis functions in the XYZ coordinates as shown in Fig. S5(c), we should make a linear transformation according to the following transformation matrix,

$$\begin{bmatrix} X_0 \\ Y_0 \\ Z_0 \end{bmatrix} = \begin{bmatrix} \frac{-1}{\sqrt{6}} & \frac{1}{\sqrt{2}} & \frac{-1}{\sqrt{3}} \\ \frac{-1}{\sqrt{6}} & \frac{-1}{\sqrt{2}} & \frac{-1}{\sqrt{3}} \\ \frac{2}{\sqrt{6}} & 0 & \frac{-1}{\sqrt{3}} \end{bmatrix} \begin{bmatrix} X \\ Y \\ Z \end{bmatrix} \tag{10}$$

Then the transformed basis functions can be expressed as following:

$$a_1 : d_{z^2} \tag{11}$$

$$e_1 \begin{cases} e_{a1} : \dfrac{1}{\sqrt{3}} d_{x^2-y^2} - \dfrac{\sqrt{2}}{\sqrt{3}} d_{xz} \\ e_{b1} : \dfrac{1}{\sqrt{3}} d_{xy} + \dfrac{\sqrt{2}}{\sqrt{3}} d_{yz} \end{cases} \tag{12}$$

$$e_2 \begin{cases} e_{a2} : \dfrac{\sqrt{2}}{\sqrt{3}} d_{x^2-y^2} + \dfrac{1}{\sqrt{3}} d_{xz} \\ e_{b2} : -\dfrac{\sqrt{2}}{\sqrt{3}} d_{xy} + \dfrac{1}{\sqrt{3}} d_{yz} \end{cases} \tag{13}$$

It can be seen that the transformed basis functions are still orthogonal to each other. We also compare our derived symmetry-adapted bases with that from density functional theory (DFT) calculation as shown in Fig. S6. We found that the shape and pointed-direction of functions from our derivation are similar to wavefunctions at Γ-point from DFT calculation. Therefore, we clarify that these basis functions of d orbitals that we chose are reasonable.

However, there are two points to be noted. First, the ratio coefficient between $d_{x^2-y^2}$ (d_{xy}) and d_{xz} (d_{yz}) from DFT calculation is not strictly equal to $\sqrt{2}(1/\sqrt{2})$ as we derive. The ratio coefficient will change with the species of transition metal atoms and are different between e_1 and e_2, which may be caused by the interaction between d-electrons themselves. Therefore, we replace the $\sqrt{2}$ with α/β and γ/δ, where $\alpha/\beta = \gamma/\delta$. This relation of equivalence is verified by the Γ-point orbital-component from DFT calculation as listed in the main text as shown in Table III. Second, the coefficients before $d_{x^2-y^2}$, d_{xy}, d_{xz}, d_{yz} from DFT calculation contain four components as shown in Table III. There is a recombination of basis functions for one e degenerated-level, which means the eigenfunctions in one e_1 (e_2) degenerated-level are the linear combinations of the two basis functions. To maintain the orthogonality of basis functions in one degenerate-level and opposite pointed direction between e_1 and e_2, we make a linear transformation of basis functions in each subgroup as following:

$$e_1^{final} \begin{cases} {e_{a1}}^{final} = e_{a1} + e_{b1} \\ {e_{b1}}^{final} = -e_{a1} + e_{b1} \end{cases} \tag{14}$$

$$e_2^{final} \begin{cases} {e_{a2}}^{final} = e_{a2} - e_{b2} \\ {e_{b2}}^{final} = e_{a2} + e_{b2} \end{cases} \tag{15}$$

Thus, the more tedious expressions are used for the derived eigenfunctions, as shown in the main text.

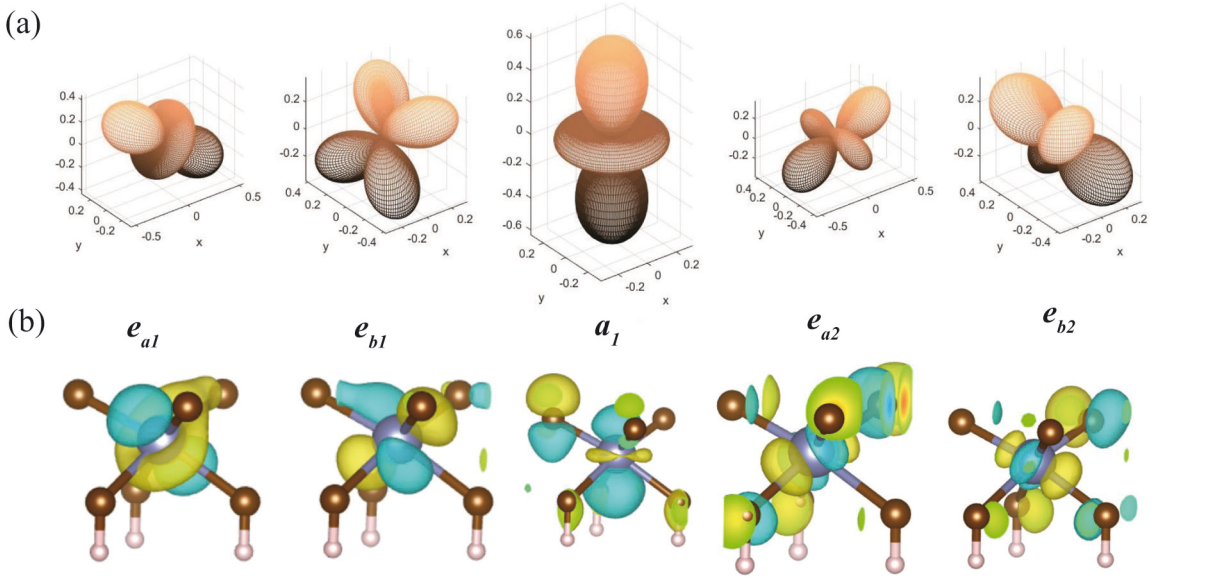

FIG. S6. (a) Schematic plot of wavefunctions of d orbitals by our derived expression. (b) Schematic plot of wavefunctions of d orbitals at Γ point from DFT calculation, where the wavefunctions are from d-electrons in spin-up channel of V cation in monolayer VOOH, and the corresponding energy could be found in Fig. S3(a).

EVALUATION OF T_C

We evaluated the value of Curie temperature T_C according to exchange parameters. The exchange parameters J are calculated according to the Heisenberg model. In our work, we only consider the nearest-neighbor and next-nearest-neighbor adjacent atoms. Then the spin-dependent Hamiltonian can be written as

$$H_{<i,j>} = -\sum_{<i,j>} J_1 \vec{S}_i \vec{S}_j - \sum_{<i,j>} J_2 \vec{S}_i \vec{S}_j \tag{16}$$

where $<i,j>$ represents the sum over all neighboring pairs in the lattice. Considering the same supercells and magnetic configurations as that in [4] as shown in Fig. 1(a), the exchange parameters J_1 and J_2 could be expressed as

$$\begin{aligned} J_1 =& \frac{1}{2}(2E_{zAFM} - E_{FM} - E_{sAFM}) \\ J_2 =& E_{sAFM} - E_{zAFM} \end{aligned} \tag{17}$$

where E_{zAFM}, E_{sAFM}, and E_{FM} are the total energies per unit cell according to zigzag, stripe antiferromagnetic and ferromagnetic configurations, respectively. The exchange parameters for monolayer VOOH and CrOOH are listed in Table S2. The value of J_2 is significantly smaller than that of J_1, so the value of Curie temperature T_C is determined mainly by the nearest-neighbor parameter J_1.

TABLE S2. Nearest-neighbor (J_1) and next-nearest-neighbor (J_2) exchange parameters for monolayer VOOH and CrOOH.

	J_1(meV)	J_2(meV)
VOOH	8.1	-1.2
CrOOH	15.5	-0.1

As we described in the main text, the magnetic easy-axis is in the 2D plane for the monolayer VOOH, indicating it as an XY magnet, while for monolayer CrOOH, the magnetic easy-axis is normal to the 2D planes. We have used two methods to discuss the value of Curie temperature T_C for the monolayer VOOH and CrOOH, respectively.

For the monolayer VOOH as the XY magnet, we evaluated the Curie temperature T_C using the expression derived from the Monte Carlo method [4]. They obtained a simple relation between exchange parameter J_1 and T_C as T_C

$= 1.335\ J_1/k_B$ for triangular lattice, where k_B is the Boltzmann constant. Therefore, the Curie temperature T_C of monolayer VOOH is estimated as 138 K.

For monolayer CrOOH with perpendicular magnetic anisotropy, we evaluated the Curie temperature based on the Weiss molecular-field theory [5–7] as

$$T_C = \frac{2zJS(S+1)}{3K_B} \tag{18}$$

where $z = 6$ is the number of nearest-neighboring atoms for monolayer CrOOH, S $= \frac{3}{2}$ is the spin quantum number of each Cr atom, and J is the exchange integral that could be obtained by

$$J = \frac{J_1}{2zS^2} \tag{19}$$

For the monolayer CrOOH, the value of the exchange integral J is 0.57 meV, and the Curie temperature T_C is about 100 K.

[1] J. S. Griffith, *The theory of transition-metal ions* (University Press, Cambridge, 1964).
[2] S. Jiang, *The theory of ferromagnetism* (Science Press, Beijing, 1993).
[3] C. Bradley and A. Cracknall, *The mathematical Theory of Symmetry in Solids: Representation Theory for Point Groups and Space Groups* (Clarendon Press, Oxford, 1972).
[4] S. Zhang, R. Xu, W. Duan, and X. Zou, Adv. Funct. Mater. **29**, 1808380 (2019).
[5] B. D. Cullity and C. D. Graham, *Introduction to Magnetic Materials, 2nd ed.* (Wiley & Sons, Inc., Hoboken, NJ, 2009).
[6] A. R. Wildes, B. Roessli, B. Lebech, and K. W. Godfrey, J. Phys.: Condens. Matter **10**, 6417 (1998).
[7] H. L. Zhuang, Y. Xie, P. R. C. Kent, and P. Ganesh, Phys. Rev. B **92**, 035407 (2015).